CMS Physics Analysis Summary

Contact: cms-pag-conveners-smp@cern.ch 2019/03/24

Measurement of the pp $\to$ ZZ production cross section at $\sqrt{s} = 13$ TeV with the Run 2 data set

The CMS Collaboration

Abstract

Four-lepton production in proton-proton collisions, pp $\to$ $(Z/\gamma^*)(Z/\gamma^*) \to 4\ell$, where ℓ = e or μ, is studied at a center-of-mass energy of 13 TeV with the CMS detector at the LHC. The data samples correspond to integrated luminosities of 41.5 and 59.7 fb^{-1}, collected in 2017 and 2018 running periods respectively. By combining the 2017 and 2018 results with the previously published 2016 results, the ZZ production cross section is measured, $\sigma_{tot}(\text{pp} \to \text{ZZ}) = 17.1 \pm 0.3(\text{stat}) \pm 0.4(\text{syst}) \pm 0.4(\text{theo}) \pm 0.3(\text{lumi})$ pb, for events with two opposite-sign, same-flavor lepton pairs produced in the mass region $60 < m_{\ell^+\ell^-} < 120$ GeV. The measured cross section value is consistent with standard model predictions.

1 Introduction

Measurements of diboson production at the CERN LHC allow precision tests of the standard model (SM). In the SM, ZZ production proceeds mainly through quark-antiquark t- and u-channel scattering diagrams. In calculations at higher orders in quantum chromodynamics (QCD), gluon-gluon fusion also contributes via box diagrams with quark loops.

Previous measurements of the ZZ production cross section for pairs of on-shell Z bosons, produced in the dilepton mass range 60–120 GeV, were performed by the CMS Collaboration with data sets corresponding to integrated luminosities of 5.1 fb^{-1} at $\sqrt{s} = 7$ TeV [1], 19.6 fb^{-1} at $\sqrt{s} = 8$ TeV [2, 3] in the $\text{ZZ} \to 2\ell 2\ell''$ and $\text{ZZ} \to 2\ell 2\nu$ decay channels, where $\ell = \text{e}$ or μ and $\ell'' = \text{e}, \mu$, or τ, and with an integrated luminosity of 2.6 fb^{-1} [4] and 35.9 fb^{-1} [5] at $\sqrt{s} = 13$ TeV in the $\text{ZZ} \to 2\ell 2\ell'$ decay channel, where $\ell' = \text{e}$ or μ. All of them agree with SM predictions. The ATLAS Collaboration produced similar results at $\sqrt{s} = 7$, 8, and 13 TeV [6–9], which also agree with the SM. These measurements are important for testing predictions that were recently made available at next-to-next-to-leading order (NNLO) in QCD [10–12].

This physics analysis summary reports a study of four-lepton production ($\text{pp} \to 2\ell 2\ell'$, where 2ℓ and $2\ell'$ indicate opposite-sign pairs of electrons or muons) at $\sqrt{s} = 13$ TeV with a data set corresponding to an integrated luminosity of 41.5 ± 1.0 and 59.7 ± 1.5 fb^{-1} recorded in 2017 and 2018. The measurements are combined with previously published results from Ref. [5], thus the total integrated luminosity of the whole sample increases to 137.4 fb^{-1}. Cross sections are measured for nonresonant production of pairs of Z bosons, $\text{pp} \to \text{ZZ}$, where both Z bosons are produced on-shell, defined as the mass range 60–120 GeV.

specify which lumi is for 2017 and 2018

2 The CMS detector

A detailed description of the CMS detector, together with a definition of the coordinate system used and the relevant kinematic variables, can be found in Ref. [13].

The central feature of the CMS apparatus is a superconducting solenoid of 6 m internal diameter, providing a magnetic field of 3.8 T. Within the solenoid volume are a silicon pixel and strip tracker, a lead tungstate crystal electromagnetic calorimeter (ECAL), and a brass and scintillator hadron calorimeter, which provide coverage in pseudorapidity $|\eta| < 1.479$ in a cylindrical barrel and $1.479 < |\eta| < 3.0$ in two endcap regions. Forward calorimeters extend the coverage provided by the barrel and endcap detectors to $|\eta| < 5.0$. Muons are measured in gas-ionization detectors embedded in the steel flux-return yoke outside the solenoid in the range $|\eta| < 2.4$, with detection planes made using three technologies: drift tubes, cathode strip chambers, and resistive plate chambers.

Electron momenta are estimated by combining energy measurements in the ECAL with momentum measurements in the tracker. The momentum resolution for electrons with transverse momentum $p_{\text{T}} \approx 45$ GeV from $\text{Z} \to \text{e}^+\text{e}^-$ decays ranges from 1.7% for nonshowering electrons in the barrel region to 4.5% for showering electrons in the endcaps [14]. Matching muons to tracks identified in the silicon tracker results in a p_{T} resolution for muons with $20 < p_{\text{T}} < 100$ GeV of 1.3–2.0% in the barrel and better than 6% in the endcaps. The p_{T} resolution in the barrel is better than 10% for muons with p_{T} up to 1 TeV [15, 16].

3 Signal and background simulation

Signal events are generated with POWHEG 2.0 [17–21] at next-to-leading order (NLO) in QCD for quark-antiquark processes and leading order (LO) for quark-gluon processes. This includes ZZ, $Z\gamma^*$, Z, $\gamma^*\gamma^*$ and SM Higgs production with a constraint of $m_{\ell\ell'} > 4\,\text{GeV}$ applied to all pairs of oppositely charged leptons at the generator level to avoid infrared divergences. The $gg \to ZZ$ process is simulated at LO with MCFM v7.0 [22]. These samples are scaled to correspond to cross sections calculated at NNLO in QCD for $q\bar{q} \to ZZ$ [10] (a scaling K factor of 1.1) and at NLO in QCD for $gg \to ZZ$ and $gg \to H$ [23] (K factor of 1.7). The Higgs boson decay is modeled with JHUGEN 3.1.8 [24–26].

Samples for background processes containing three or four prompt leptons in the final state, like $t\bar{t}Z$, WWZ and WZ production, are produced with MADGRAPH5_aMC@NLO v2.4.2 [27].

The PYTHIA v8.175 [20, 28, 29] package is used for parton showering, hadronization, and the underlying event simulation, with parameters set by the CP5 tune [30]. The NNPDF 31_nnlo_as_0118 and NNPDF31_lo_as_0130 [31] sets are used as the default sets of parton distribution functions (PDFs).

The detector response is simulated using a detailed description of the CMS detector implemented with the GEANT4 package [32]. The event reconstruction is performed with the same algorithms used for data. The simulated samples include additional interactions per bunch crossing, referred to as pileup. The simulated events are weighted so that the pileup distribution matches the data.

4 Event reconstruction

All long-lived particles—electrons, muons, photons, and charged and neutral hadrons—in each collision event are identified and reconstructed with the CMS particle-flow (PF) algorithm [33] from a combination of the signals from all subdetectors. Reconstructed electrons [14] and muons [15] are considered candidates for inclusion in four-lepton final states if they have $p_T^e > 7\,\text{GeV}$ and $|\eta^e| < 2.5$ or $p_T^\mu > 5\,\text{GeV}$ and $|\eta^\mu| < 2.4$.

Lepton candidates are also required to originate from the event vertex, defined as the reconstructed proton-proton interaction vertex with the largest value of summed physics object p_T^2. The physics objects used in the event vertex definition are the objects returned by a jet finding algorithm [34, 35] applied to all charged tracks associated with the vertex, plus the corresponding associated missing transverse momentum [36]. The distance of closest approach between each lepton track and the event vertex is required to be less than 0.5 cm in the plane transverse to the beam axis, and less than 1 cm in the direction along the beam axis. Furthermore, the significance of the three-dimensional impact parameter relative to the event vertex, SIP_{3D}, is required to satisfy $\text{SIP}_{3D} \equiv |\text{IP}/\sigma_{\text{IP}}| < 4$ for each lepton, where IP is the distance of closest approach of each lepton track to the event vertex and σ_{IP} is its associated uncertainty.

Lepton candidates are required to be isolated from other particles in the event. The relative isolation is defined as

$$R_{\text{iso}} = \left[\sum_{\substack{\text{charged}\\ \text{hadrons}}} p_T + \max\left(0, \sum_{\substack{\text{neutral}\\ \text{hadrons}}} p_T + \sum_{\text{photons}} p_T - p_T^{\text{PU}}\right) \right] \Big/ p_T^\ell, \tag{1}$$

where the sums run over the charged and neutral hadrons and photons identified by the PF algorithm, in a cone defined by $\Delta R \equiv \sqrt{(\Delta\eta)^2 + (\Delta\phi)^2} < 0.3$ around the lepton trajectory.

Here ϕ is the azimuthal angle in radians. To minimize the contribution of charged particles from pileup to the isolation calculation, charged hadrons are included only if they originate from the event vertex. The contribution of neutral particles from pileup is $p_{\mathrm{T}}^{\mathrm{PU}}$. For electrons, $p_{\mathrm{T}}^{\mathrm{PU}}$ is evaluated with the "jet area" method described in Ref. [37]; for muons, it is taken to be half the sum of the p_{T} of all charged particles in the cone originating from pileup vertices. The factor one-half accounts for the expected ratio of charged to neutral particle energy in hadronic interactions. A lepton is considered isolated if $R_{\mathrm{iso}} < 0.35$.

The lepton reconstruction, identification, and isolation efficiencies are measured with a "tag-and-probe" technique [38] applied to a sample of $\mathrm{Z} \to \ell^+\ell^-$ data events. The measurements are performed in several bins of p_{T}^{ℓ} and $|\eta^{\ell}|$. The electron reconstruction and selection efficiency in the ECAL barrel (endcaps) varies from about 85% (77%) at $p_{\mathrm{T}}^{\mathrm{e}} \approx 10\,\mathrm{GeV}$ to about 95% (89%) for $p_{\mathrm{T}}^{\mathrm{e}} \geq 20\,\mathrm{GeV}$, while in the barrel-endcap transition region this efficiency is about 85% averaged over all electrons with $p_{\mathrm{T}}^{\mathrm{e}} > 7\,\mathrm{GeV}$. The muons are reconstructed and identified with efficiencies above ~98% within $|\eta^{\mu}| < 2.4$.

5 Event selection

The primary triggers for this analysis require the presence of a pair of loosely isolated leptons of the same or different flavors [39]. The highest p_{T} lepton must have $p_{\mathrm{T}}^{\ell} > 17\,\mathrm{GeV}$, and the subleading lepton must have $p_{\mathrm{T}}^{\mathrm{e}} > 12\,\mathrm{GeV}$ if it is an electron or $p_{\mathrm{T}}^{\mu} > 8\,\mathrm{GeV}$ if it is a muon. The tracks of the triggering leptons are required to originate within 2 mm of each other in the plane transverse to the beam axis. Triggers requiring a triplet of lower-p_{T} leptons with no isolation criterion, or a single high-p_{T} electron or muon, are also used. An event is used if it passes any trigger regardless of the decay channel. The total trigger efficiency for events within the acceptance of this analysis is greater than 98%.

The four-lepton candidate selections are based on those used in Ref. [40]. A signal event must contain at least two Z/γ^* candidates, each formed from an oppositely charged pair of isolated electron candidates or muon candidates. Among the four leptons, the highest p_{T} lepton must have $p_{\mathrm{T}} > 20\,\mathrm{GeV}$, and the second-highest p_{T} lepton must have $p_{\mathrm{T}}^{\mathrm{e}} > 12\,\mathrm{GeV}$ if it is an electron or $p_{\mathrm{T}}^{\mu} > 10\,\mathrm{GeV}$ if it is a muon. All leptons are required to be separated from each other by $\Delta R\,(\ell_1, \ell_2) > 0.02$, and electrons are required to be separated from muons by $\Delta R\,(\mathrm{e}, \mu) > 0.05$.

Within each event, all permutations of leptons giving a valid pair of Z/γ^* candidates are considered separately. Within each 4ℓ candidate, the dilepton candidate with an invariant mass closest to 91.2 GeV, taken as the nominal Z boson mass [41], is denoted Z_1 and is required to have a mass greater than 40 GeV. The other dilepton candidate is denoted Z_2. Both m_{Z_1} and m_{Z_2} are required to be less than 120 GeV. All pairs of oppositely charged leptons in the 4ℓ candidate are required to have $m_{\ell\ell'} > 4\,\mathrm{GeV}$ regardless of their flavor.

If multiple 4ℓ candidates within an event pass all selections, the one with m_{Z_1} closest to the nominal Z boson mass is chosen. In the rare case of further ambiguity, which may arise in less than 0.5% of events when five or more passing lepton candidates are found, the Z_2 candidate that maximizes the scalar p_{T} sum of the four leptons is chosen.

The $\mathrm{pp} \to \mathrm{ZZ}$ cross section is measured using events where both m_{Z_1} and m_{Z_2} are greater than 60 GeV. Decays of the Z bosons to τ leptons with subsequent decays to electrons and muons are heavily suppressed by requirements on lepton p_{T}, and the contribution of such events is less than 0.5% of the total ZZ yield. If these events pass the selection requirements of the analysis, they are considered signal, while they are not considered at generator level in the cross section

measurement procedure. Thus, the correction for possible τ decays is included in the efficiency calculation. The same is done for expected small contribution of the Higgs events.

6 Background estimation

The major background contributions arise from Z boson and WZ diboson production in association with jets and from $\mathrm{t\bar{t}}$ production. In all these cases, particles from jet fragmentation satisfy both lepton identification and isolation criteria, and are thus misidentified as signal leptons.

The probability for such objects to be selected is measured from a sample of $\mathrm{Z} + \ell_{\text{candidate}}$ events, where Z denotes a pair of oppositely charged, same-flavor leptons that pass all analysis requirements and satisfy $|m_{\ell^+\ell^-} - m_{\mathrm{Z}}| < 10\,\text{GeV}$, where m_{Z} is the nominal Z boson mass. Each event in this sample must have exactly one additional object $\ell_{\text{candidate}}$ that passes relaxed identification requirements with no isolation requirements applied. The misidentification probability for each lepton flavor, measured in bins of lepton candidate p_{T} and η, is defined as the ratio of the number of candidates that pass the final isolation and identification requirements to the total number in the sample. The number of $\mathrm{Z} + \ell_{\text{candidate}}$ events is corrected for the contamination from WZ production and ZZ production in which one lepton is not reconstructed. These events have a third genuine, isolated lepton that must be excluded from the misidentification probability calculation. The WZ contamination is suppressed by requiring the missing transverse momentum $p_{\mathrm{T}}^{\text{miss}}$ to be below 25 GeV. The $p_{\mathrm{T}}^{\text{miss}}$ is defined as the magnitude of the missing transverse momentum vector $\vec{p}_{\mathrm{T}}^{\,\text{miss}}$, the projection onto the plane transverse to the beams of the negative vector sum of the momenta of all reconstructed PF candidates in the event, corrected for the jet energy scale. Additionally, the transverse mass calculated with $\vec{p}_{\mathrm{T}}^{\,\text{miss}}$ and the $\vec{p}_{\mathrm{T}}$ of $\ell_{\text{candidate}}$, $m_{\mathrm{T}} \equiv \sqrt{(p_{\mathrm{T}}^{\ell} + p_{\mathrm{T}}^{\text{miss}})^2 - (\vec{p}_{\mathrm{T}}^{\,\ell} + \vec{p}_{\mathrm{T}}^{\,\text{miss}})^2}$, is required to be less than 30 GeV. The residual contribution of WZ and ZZ events, which may be up to a few percent of the events with $\ell_{\text{candidate}}$ passing all selection criteria, is estimated from simulation and subtracted.

To account for all sources of background events, two control samples are used to estimate the number of background events in the signal regions. Both are defined to contain events with a dilepton candidate satisfying all requirements (Z_1) and two additional lepton candidates $\ell^+\ell^-$. In one control sample, enriched in WZ events, one ℓ candidate is required to satisfy the full identification and isolation criteria and the other must fail the full criteria and instead satisfy only the relaxed ones; in the other, enriched in Z+jets events, both ℓ candidates must satisfy the relaxed criteria, but fail the full criteria. The additional leptons must have opposite charge and the same flavor ($\mathrm{e^{\pm}e^{\mp}}$, $\mu^{\pm}\mu^{\mp}$). From this set of events, the expected number of background events in the signal region, denoted "Z + X" in the figures, is obtained by scaling the number of observed $\mathrm{Z}_1 + \ell^+\ell^-$ events by the misidentification probability for each lepton failing the selection. It is found to be approximately 4% of the total expected yield. The procedure is described in more detail in Ref. [40].

In addition to these nonprompt backgrounds, $\mathrm{t\bar{t}Z}$ and WWZ processes contribute a smaller number of events with four prompt leptons, which is estimated from simulated samples to be around 1% of the expected $\mathrm{ZZ} \to 4\ell$ yield. The total background contributions to the $\mathrm{ZZ} \to 4\ell$ signal regions are summarized in Section 8.

7 Systematic uncertainties

The major sources of systematic uncertainty and their effect on the measured cross sections are summarized in Table 1. In both data and simulated event samples, trigger efficiencies are eval-

uated with a tag-and-probe technique. The ratio of data to simulation is applied to simulated events, and the size of the resulting change in expected yield is taken as the uncertainty in the determination of the trigger efficiency. This uncertainty is around 2% of the final estimated yield.

Table 1: The contributions of each source of systematic uncertainty in the cross section measurements. The integrated luminosity uncertainty, and the PDF and scale uncertainties, are considered separately. All other uncertainties are added in quadrature into a single systematic uncertainty. Uncertainties that vary by decay channel are listed as a range.

Uncertainty	Range of values
Lepton efficiency	2–8%
Trigger efficiency	1–2%
Background	0.6–1.3%
Pileup	1%
PDF	1%
μ_R, μ_F	1%
Integrated luminosity	2.3% (2017) 2.5% (2018)

The lepton identification, isolation, and track reconstruction efficiencies in simulation are corrected with scaling factors derived with a tag-and-probe method and applied as a function of lepton p_T and η. To estimate the uncertainties associated with the tag-and-probe technique, the total yield is recomputed with the scaling factors varied up and down by the tag-and-probe fit uncertainties. The uncertainties associated with lepton efficiency in the $ZZ \to 4\ell$ signal regions are found to be 5% in the 4e, 3% in the 2e2μ, and 2% in the 4μ final states.

Uncertainties due to the effect of factorization (μ_F) and renormalization (μ_R) scale choices on the $ZZ \to 4\ell$ acceptance are evaluated with POWHEG and MCFM by varying the scales up and down by a factor of two with respect to the default values $\mu_F = \mu_R = m_{ZZ}$. All combinations are considered except those in which μ_F and μ_R differ by a factor of four. Parametric uncertainties (PDF+α_s) are evaluated according to the PDF4LHC prescription [42] in the acceptance calculation, and with NNPDF3.0 [43] in the cross section calculations. An additional theoretical uncertainty arises from scaling the POWHEG $q\bar{q} \to ZZ$ simulated sample from its NLO cross section to the NNLO prediction, and the MCFM $gg \to ZZ$ samples from their LO cross sections to the NLO predictions. The change in the acceptance corresponding to this scaling procedure is found to be 1.1%. All these theoretical uncertainties are added in quadrature.

The largest uncertainty in the estimated background yield arises from differences in sample composition between the $Z + \ell_{\text{candidate}}$ control sample used to calculate the lepton misidentification probability and the $Z + \ell^+\ell^-$ control sample. A further uncertainty arises from the limited number of events in the $Z + \ell_{\text{candidate}}$ sample. A systematic uncertainty of 40% is applied to the lepton misidentification probability to cover both effects. The size of this effect varies by channel, but is of the order of 1% of the total expected yield.

The uncertainty in the integrated luminosity of the data samples is 2.3% [44] (2017) and 2.5% (2018).

8 Cross section measurement

The distribution of invariant mass of ZZ system, individual mass of reconstructed Z boson candidates in ZZ events, and their correspondent p_T distributions are shown in Fig. 1. The p_T and η distributions for individual leptons are shown in Fig. 2. These distributions are shown for

data and Monte Carlo to allow comparison to SM expectations. The expectations include the non-resonant ZZ predictions normalized to the NNLO cross sections and the standard model Higgs boson with mass 125 GeV production. The reducible background estimated from data is also shown. The measured and expected event yields for all decay channels for on-shell measurement are summarized in Table 2.

The measured yields are used to evaluate the ZZ production cross section in the fiducial phase space. The signal acceptance is evaluated from simulation and corrected for each individual lepton flavor in bins of p_{T} and η using factors obtained with the tag-and-probe technique. The branching fraction $BR_{\mathrm{Z}\to\ell\ell}$ is $3.3658 \pm 0.0023\%$ for each lepton flavor [41].

To include all final states in the cross section calculation a simultaneous fit on the number of observed events in all decay channels is performed. The likelihood is written as a combination of individual channel likelihoods for the signal and background hypotheses with the statistical and systematic uncertainties in form of the scaling nuisance parameters. The combination of different data taking periods is performed considering the theoretical uncertainties fully correlated among different periods, while the experimental uncertainties are either correlated or uncorrelated depending on their origin.

Table 2: The observed and expected yields of ZZ events, and estimated yields of background events, shown for each final state and summed in the total expected yield. First uncertainty is statistical, second is systematic. The uncertainties listed as 0.0 are less than 0.1.

Process	eeee	ee$\mu\mu$	$\mu\mu\mu\mu$	4ℓ
	2017			
VVV	$2.9 \pm 0.0 \pm 0.1$	$8.2 \pm 0.0 \pm 0.2$	$4.7 \pm 0.0 \pm 0.1$	$15.7 \pm 0.0 \pm 0.3$
Nonprompt	$4.3 \pm 0.0 \pm 1.2$	$6.9 \pm 0.0 \pm 1.1$	$4.8 \pm 0.0 \pm 1.6$	$16.0 \pm 0.0 \pm 2.3$
qqZZ	$163.4 \pm 4.7 \pm 5.1$	$418.8 \pm 8.4 \pm 5.0$	$268.1 \pm 7.5 \pm 6.6$	$850.4 \pm 12.2 \pm 9.7$
ggZZ	$32.5 \pm 0.9 \pm 1.0$	$86.6 \pm 1.7 \pm 1.0$	$54.4 \pm 1.5 \pm 1.3$	$173.6 \pm 2.5 \pm 2.0$
HZZ	$0.3 \pm 0.0 \pm 0.0$	$0.9 \pm 0.0 \pm 0.0$	$0.6 \pm 0.0 \pm 0.0$	$1.8 \pm 0.0 \pm 0.0$
Total expected	$203 \pm 6 \pm 6$	$522 \pm 10 \pm 6$	$333 \pm 9 \pm 8$	$1057 \pm 15 \pm 12$
Data	190	537	330	1057
	2018			
VVV	$4.3 \pm 0.0 \pm 0.2$	$12.0 \pm 0.0 \pm 0.3$	$6.7 \pm 0.0 \pm 0.1$	$23.0 \pm 0.0 \pm 0.4$
Nonprompt	$6.1 \pm 0.0 \pm 1.7$	$12.9 \pm 0.0 \pm 1.8$	$6.3 \pm 0.0 \pm 2.2$	$25.3 \pm 0.0 \pm 3.3$
qqZZ	$246.1 \pm 5.8 \pm 8.1$	$617.9 \pm 10.3 \pm 6.2$	$387.1 \pm 9.0 \pm 10.7$	$1251.1 \pm 14.8 \pm 14.8$
ggZZ	$49.3 \pm 1.2 \pm 1.5$	$127.4 \pm 2.1 \pm 1.3$	$78.3 \pm 1.8 \pm 2.2$	$255.1 \pm 3.0 \pm 3.0$
HZZ	$0.5 \pm 0.0 \pm 0.0$	$1.3 \pm 0.0 \pm 0.0$	$0.8 \pm 0.0 \pm 0.0$	$2.6 \pm 0.0 \pm 0.0$
Total expected	$306 \pm 7 \pm 10$	$772 \pm 12 \pm 7$	$479 \pm 11 \pm 13$	$1557 \pm 18 \pm 18$
Data	303	772	482	1557

The fiducial phase spaces for the ZZ $\to 4\ell$ cross section measurements is defined as: $p_{\mathrm{T}}^{\ell_1} > 20\,\mathrm{GeV}$, $p_{\mathrm{T}}^{\ell_2} > 10\,\mathrm{GeV}$, $p_{\mathrm{T}}^{\ell_{3,4}} > 5\,\mathrm{GeV}$, $|\eta^{\ell}| < 2.5$, $m_{\ell\ell} > 4\,\mathrm{GeV}$ (any opposite-sign same-flavor pair), $60 < m_{\mathrm{Z}_1}, m_{\mathrm{Z}_2} < 120\,\mathrm{GeV}$. The generator-level leptons used for the fiducial cross section calculation are "dressed" by adding the momenta of generator-level photons within $\Delta R\,(\ell, \gamma) < 0.1$ to their momenta.

The measured ZZ fiducial cross section presented in Tab. 3 can be compared to $34.4^{+0.7}_{-0.6} \pm 0.5\,\mathrm{fb}$ calculated with POWHEG and MCFM using the same settings as the simulated samples without scaling K factors applied. The first uncertainty corresponds to PDF and second to the scales variation, as described above. The POWHEG calculations used dynamic scales $\mu_{\mathrm{F}} = \mu_{\mathrm{R}} = m_{4\ell}$, while the contribution from MCFM was computed with dynamic scales $\mu_{\mathrm{F}} = \mu_{\mathrm{R}} = 0.5 m_{4\ell}$.

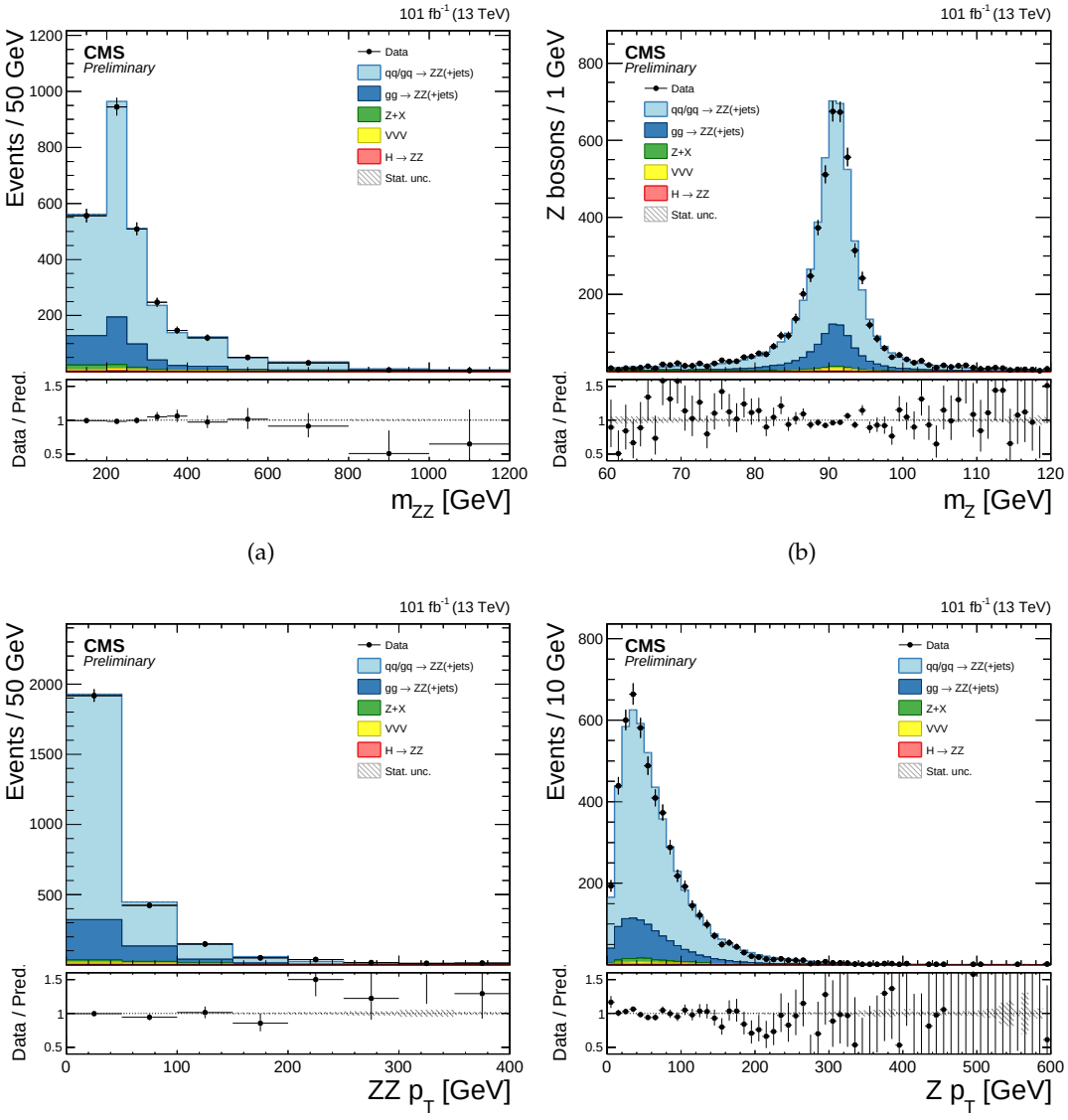

Figure 1: Distributions of (a) m_{ZZ} for ZZ events with $60 < m_{Z_1,Z_2} < 120\,\text{GeV}$; (b) mass of selected Z boson candidates; (c) transverse momentum of the ZZ system ; (d) transverse momentum of individual Z boson candidates. All decay channels for both 2017 and 2018 data taking periods are added together. The results correspond to an integrated luminosity of $101.2\,\text{fb}^{-1}$. Points represent the data, shaded histograms represent the expected standard model predictions and reducible background estimated from data.

Table 3: The measured fiducial cross section for each data sample, and combined. The published result from Ref. [5] is also included.

Year	Fiducial cross section, fb
2016 [5]	$40.9 \pm 1.3\,(\text{stat}) \pm 1.4\,(\text{syst}) \pm 1.0\,(\text{lumi})$
2017	$39.1 \pm 1.2\,(\text{stat}) \pm 1.2\,(\text{syst}) \pm 1.0\,(\text{lumi})$
2018	$39.2 \pm 1.0\,(\text{stat}) \pm 1.3\,(\text{syst}) \pm 1.0\,(\text{lumi})$
Combined	$39.9 \pm 0.7\,(\text{stat}) \pm 1.0\,(\text{syst}) \pm 0.7\,(\text{lumi})$

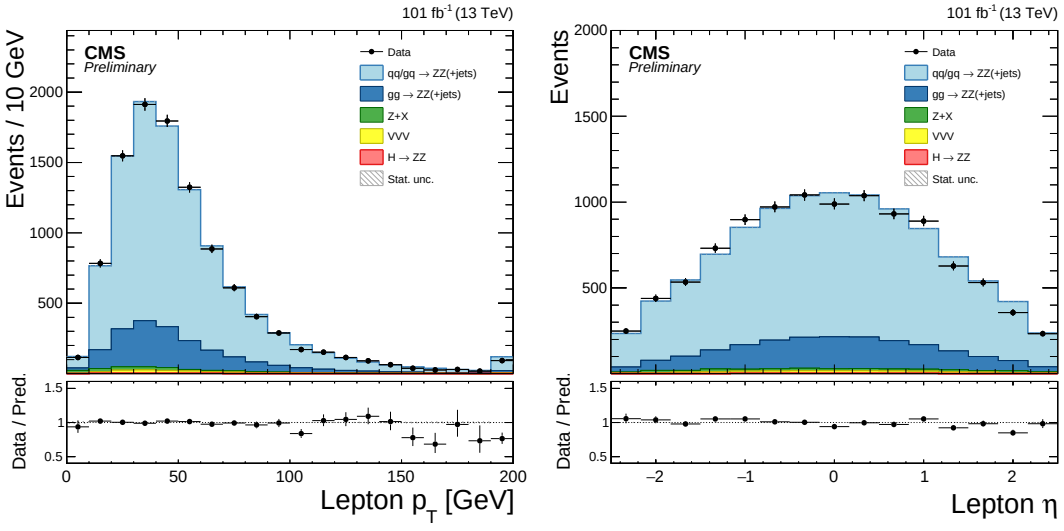

(a) (b)

Figure 2: Distributions of (a) transverse momentum and (b) pseudorapidity for individual leptons. The results correspond to an integrated luminosity of 101.2 fb^{-1}. Points represent the data, shaded histograms represent the expected standard model predictions and reducible background estimated from data.

Table 4: The measured total $\sigma(\text{pp} \to \text{ZZ})$ cross section for each data sample, and combined. The published result from Ref. [5] is also included.

Year	Total cross section, pb
2016 [5]	$17.5^{+0.6}_{-0.5}\,(\text{stat}) \pm 0.6\,(\text{syst}) \pm 0.4\,(\text{theo}) \pm 0.4\,(\text{lumi})$
2017	$16.8 \pm 0.5\,(\text{stat}) \pm 0.5\,(\text{syst}) \pm 0.4\,(\text{theo}) \pm 0.4\,(\text{lumi})$
2018	$16.8 \pm 0.4\,(\text{stat}) \pm 0.6\,(\text{syst}) \pm 0.4\,(\text{theo}) \pm 0.4\,(\text{lumi})$
Combined	$17.1 \pm 0.3\,(\text{stat}) \pm 0.4\,(\text{syst}) \pm 0.4\,(\text{theo}) \pm 0.3\,(\text{lumi})$

The total ZZ production cross section for both dileptons produced in the mass range 60–120 GeV and $m_{\ell^+\ell'^-} > 4$ GeV is presented in Tab. 4. The measured total cross section can be compared to the theoretical value of $14.5^{+0.5}_{-0.4} \pm 0.2$ pb calculated with a combination of POWHEG and MCFM with the same settings as described for $\sigma_{\text{fid}}(\text{pp} \to \text{ZZ} \to 4\ell)$. It can also be compared to $16.2^{+0.6}_{-0.4}$ pb, calculated at NNLO in QCD via MATRIX v1.0.0_beta4 [10–12], or $15.0^{+0.7}_{-0.6} \pm 0.2$ pb, calculated with MCFM at NLO in QCD with additional contributions from LO $\text{gg} \to \text{ZZ}$ diagrams. Both values are calculated with the NNPDF3.0 PDF sets, at NNLO and NLO, respectively, and fixed scales set to $\mu_{\text{F}} = \mu_{\text{R}} = m_{\text{Z}}$.

The total ZZ cross section is shown in Fig. 3 as a function of the proton-proton center-of-mass energy. Results from CMS [1, 2] and ATLAS [6, 7, 9] are compared to predictions from MATRIX and MCFM with the NNPDF3.0 PDF sets and fixed scales $\mu_{\text{F}} = \mu_{\text{R}} = m_{\text{Z}}$. The MATRIX prediction uses PDFs calculated at NNLO, while the MCFM prediction uses NLO PDFs. The uncertainties are statistical (inner bars) and statistical and systematic added in quadrature (outer bars). The band around the MATRIX predictions reflects scale uncertainties, while the band around the MCFM predictions reflects both scale and PDF uncertainties.

9 Summary

Four-lepton production in proton-proton collisions, $\text{pp} \to (\text{Z}/\gamma^*)(\text{Z}/\gamma^*) \to 4\ell$, where $\ell = \text{e}$ or μ, was studied at a center-of-mass energy of 13 TeV with the CMS detector at the LHC. The data sample corresponds to an integrated luminosity of 41.5 fb^{-1} and 59.7 fb^{-1}, collected in 2017 and 2018 running periods respectively. By combining the 2017 and 2018 results with the previously published 2016 results, the ZZ production cross section was measured, $\sigma_{tot}(pp \to ZZ) = 17.1 \pm 0.3\,(\text{stat}) \pm 0.4\,(\text{syst}) \pm 0.4\,(\text{theo}) \pm 0.3\,(\text{lumi})$ pb, for events with two opposite-sign, same-flavor lepton pairs produced in the mass region $60 < m_{\ell^+\ell^-} < 120$ GeV. Measured cross section value is consistent with the standard model predictions.

References

[1] CMS Collaboration, "Measurement of the ZZ production cross section and search for anomalous couplings in $2\ell 2\ell'$ final states in pp collisions at $\sqrt{s} = 7$ TeV", *JHEP* **01** (2013) 063, doi:10.1007/JHEP01(2013)063, arXiv:1211.4890.

[2] CMS Collaboration, "Measurement of the $\text{pp} \to \text{ZZ}$ production cross section and constraints on anomalous triple gauge couplings in four-lepton final states at $\sqrt{s} = 8$ TeV", *Phys. Lett. B* **740** (2015) 250, doi:10.1016/j.physletb.2014.11.059, arXiv:1406.0113. [Corrigenum: doi:10.1016/j.physletb.2016.04.010].

[3] CMS Collaboration, "Measurements of the ZZ production cross sections in the $2\ell 2\nu$ channel in proton-proton collisions at $\sqrt{s} = 7$ and 8 TeV and combined constraints on triple gauge couplings", *Eur. Phys. J. C* **75** (2015) 511, doi:10.1140/epjc/s10052-015-3706-0, arXiv:1503.05467.

[4] CMS Collaboration, "Measurement of the ZZ production cross section and $\text{Z} \to \ell^+\ell^-\ell'^+\ell'^-$ branching fraction in pp collisions at $\sqrt{s} = 13$ TeV", *Phys. Lett. B* **763** (2016) 280, doi:10.1016/j.physletb.2016.10.054, arXiv:1607.08834.

[5] CMS Collaboration, "Measurements of the $\text{pp} \to \text{ZZ}$ production cross section and the $\text{Z} \to 4\ell$ branching fraction, and constraints on anomalous triple gauge couplings at $\sqrt{s} = 13$ TeV", *Eur. Phys. J. C* **78** (2018) 165, doi:10.1140/epjc/

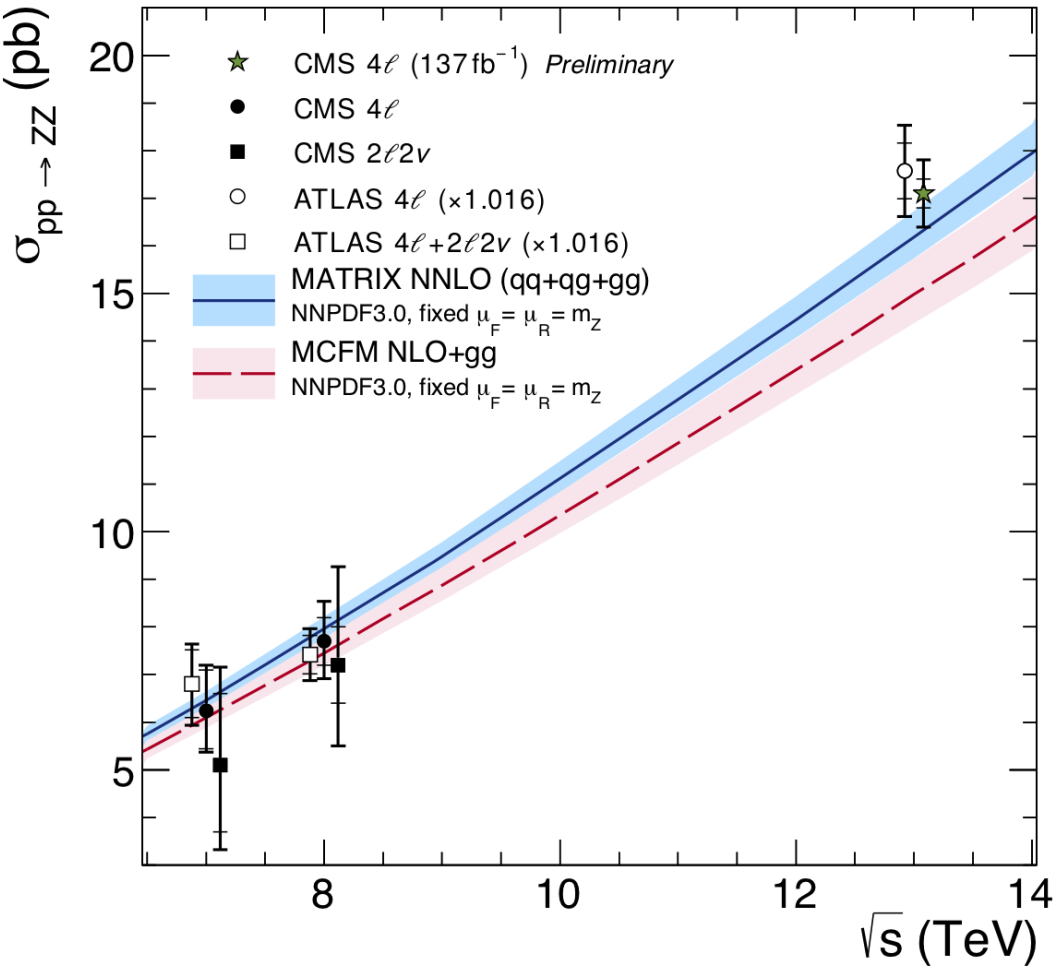

Figure 3: The total ZZ cross section as a function of the proton-proton center-of-mass energy. Results from the CMS and ATLAS experiments are compared to predictions from MATRIX at NNLO in QCD, and MCFM at NLO in QCD. The MCFM prediction also includes gluon-gluon initiated production at LO in QCD. Both predictions use NNPDF3.0 PDF sets and fixed scales $\mu_F = \mu_R = m_Z$. Details of the calculations and uncertainties are given in the text. The ATLAS measurements were performed with a Z boson mass window of 66–116 GeV, instead of 60–120 GeV used by CMS, and are corrected for the resulting 1.6% difference in acceptance. Measurements at the same center-of-mass energy are shifted slightly along the horizontal axis for clarity.

s10052-018-5567-9, 10.1140/epjc/s10052-018-5769-1, arXiv:1709.08601. [Erratum: Eur. Phys. J.C78,no.6,515(2018)].

[6] ATLAS Collaboration, "Measurement of ZZ production in pp collisions at $\sqrt{s} = 7$ TeV and limits on anomalous ZZZ and ZZγ couplings with the ATLAS detector", *JHEP* **03** (2013) 128, doi:10.1007/JHEP03(2013)128, arXiv:1211.6096.

[7] ATLAS Collaboration, "Measurements of four-lepton production in pp collisions at $\sqrt{s} = 8$ TeV with the ATLAS detector", *Phys. Lett. B* **753** (2016) 552, doi:10.1016/j.physletb.2015.12.048, arXiv:1509.07844.

[8] ATLAS Collaboration, "Measurement of the ZZ production cross section in pp collisions at $\sqrt{s} = 13$ TeV with the ATLAS detector", *Phys. Rev. Lett.* **116** (2016) 101801, doi:10.1103/PhysRevLett.116.101801, arXiv:1512.05314.

[9] ATLAS Collaboration, "$ZZ \to \ell^+\ell^-\ell'^+\ell'^-$ cross-section measurements and search for anomalous triple gauge couplings in 13 TeV pp collisions with the ATLAS detector", *Phys. Rev. D* **97** (2018) 032005, doi:10.1103/PhysRevD.97.032005, arXiv:1709.07703.

[10] F. Cascioli et al., "ZZ production at hadron colliders in NNLO QCD", *Phys. Lett. B* **735** (2014) 311, doi:10.1016/j.physletb.2014.06.056, arXiv:1405.2219.

[11] M. Grazzini, S. Kallweit, and D. Rathlev, "ZZ production at the LHC: fiducial cross sections and distributions in NNLO QCD", *Phys. Lett. B* **750** (2015) 407, doi:10.1016/j.physletb.2015.09.055, arXiv:1507.06257.

[12] M. Grazzini, S. Kallweit, and M. Wiesemann, "Fully differential NNLO computations with MATRIX", *Eur. Phys. J. C* **78** (2018), no. 7, 537, doi:10.1140/epjc/s10052-018-5771-7, arXiv:1711.06631.

[13] CMS Collaboration, "The CMS experiment at the CERN LHC", *JINST* **3** (2008) S08004, doi:10.1088/1748-0221/3/08/S08004.

[14] CMS Collaboration, "Performance of electron reconstruction and selection with the CMS detector in proton-proton collisions at $\sqrt{s} = 8$ TeV", *JINST* **10** (2015) P06005, doi:10.1088/1748-0221/10/06/P06005, arXiv:1502.02701.

[15] CMS Collaboration, "Performance of CMS muon reconstruction in pp collision events at $\sqrt{s} = 7$ TeV", *JINST* **7** (2012) P10002, doi:10.1088/1748-0221/7/10/P10002, arXiv:1206.4071.

[16] CMS Collaboration, "Performance of the CMS muon detector and muon reconstruction with proton-proton collisions at $\sqrt{s} = 13$ TeV", *JINST* **13** (2018), no. 06, P06015, doi:10.1088/1748-0221/13/06/P06015, arXiv:1804.04528.

[17] S. Alioli, P. Nason, C. Oleari, and E. Re, "NLO vector-boson production matched with shower in POWHEG", *JHEP* **07** (2008) 060, doi:10.1088/1126-6708/2008/07/060, arXiv:0805.4802.

[18] P. Nason, "A new method for combining NLO QCD with shower Monte Carlo algorithms", *JHEP* **11** (2004) 040, doi:10.1088/1126-6708/2004/11/040, arXiv:hep-ph/0409146.

[19] S. Frixione, P. Nason, and C. Oleari, "Matching NLO QCD computations with parton shower simulations: the POWHEG method", *JHEP* **11** (2007) 070, doi:10.1088/1126-6708/2007/11/070, arXiv:0709.2092.

[20] S. Alioli, P. Nason, C. Oleari, and E. Re, "A general framework for implementing NLO calculations in shower Monte Carlo programs: the POWHEG BOX", *JHEP* **06** (2010) 043, doi:10.1007/JHEP06(2010)043, arXiv:1002.2581.

[21] T. Melia, P. Nason, R. Rontsch, and G. Zanderighi, "W^+W^-, WZ and ZZ production in the POWHEG BOX", *JHEP* **11** (2011) 078, doi:10.1007/JHEP11(2011)078, arXiv:1107.5051.

[22] J. M. Campbell and R. K. Ellis, "MCFM for the Tevatron and the LHC", *Nucl. Phys. B Proc. Suppl.* **10** (2010) 205, doi:10.1016/j.nuclphysbps.2010.08.011, arXiv:1007.3492.

[23] F. Caola, K. Melnikov, R. Röntsch, and L. Tancredi, "QCD corrections to ZZ production in gluon fusion at the LHC", *Phys. Rev. D* **92** (2015) 094028, doi:10.1103/PhysRevD.92.094028, arXiv:1509.06734.

[24] Y. Gao et al., "Spin determination of single-produced resonances at hadron colliders", *Phys. Rev. D* **81** (2010) 075022, doi:10.1103/PhysRevD.81.075022, arXiv:1001.3396.

[25] S. Bolognesi et al., "Spin and parity of a single-produced resonance at the LHC", *Phys. Rev. D* **86** (2012) 095031, doi:10.1103/PhysRevD.86.095031, arXiv:1208.4018.

[26] I. Anderson et al., "Constraining anomalous HVV interactions at proton and lepton colliders", *Phys. Rev. D* **89** (2014) 035007, doi:10.1103/PhysRevD.89.035007, arXiv:1309.4819.

[27] J. Alwall et al., "The automated computation of tree-level and next-to-leading order differential cross sections, and their matching to parton shower simulations", *JHEP* **07** (2014) 079, doi:10.1007/JHEP07(2014)079, arXiv:1405.0301.

[28] T. Sjöstrand, S. Mrenna, and P. Skands, "PYTHIA 6.4 physics and manual", *JHEP* **05** (2006) 026, doi:10.1088/1126-6708/2006/05/026, arXiv:hep-ph/0603175.

[29] T. Sjöstrand et al., "An introduction to PYTHIA 8.2", *Comput. Phys. Commun.* **191** (2015) 159, doi:10.1016/j.cpc.2015.01.024, arXiv:1410.3012.

[30] CMS Collaboration, "Extraction and validation of a new set of CMS PYTHIA8 tunes from underlying-event measurements", Technical Report CMS-PAS-GEN-17-001, CERN, Geneva, 2018.

[31] NNPDF Collaboration, "Parton distributions from high-precision collider data", *Eur. Phys. J. C.* **77** (2017) 663, doi:10.1140/epjc/s10052-017-5199-5, arXiv:1706.00428.

[32] GEANT4 Collaboration, "GEANT4—a simulation toolkit", *Nucl. Instrum. Meth. A* **506** (2003) 250, doi:10.1016/S0168-9002(03)01368-8.

[33] CMS Collaboration, "Particle-flow reconstruction and global event description with the CMS detector", *JINST* **12** (2017) P10003, doi:10.1088/1748-0221/12/10/P10003, arXiv:1706.04965.

[34] M. Cacciari, G. P. Salam, and G. Soyez, "The Anti-k_t jet clustering algorithm", *JHEP* **04** (2008) 063, doi:10.1088/1126-6708/2008/04/063, arXiv:0802.1189.

[35] M. Cacciari, G. P. Salam, and G. Soyez, "FastJet user manual", *Eur. Phys. J. C* **72** (2012) 1896, doi:10.1140/epjc/s10052-012-1896-2, arXiv:1111.6097.

[36] CMS Collaboration, "Technical proposal for the phase-II upgrade of the Compact Muon Solenoid", CMS Technical proposal CERN-LHCC-2015-010, CMS-TDR-15-02, CERN, 2015.

[37] M. Cacciari and G. P. Salam, "Pileup subtraction using jet areas", *Phys. Lett. B* **659** (2008) 119, doi:10.1016/j.physletb.2007.09.077, arXiv:0707.1378.

[38] CMS Collaboration, "Measurement of the inclusive W and Z production cross sections in pp collisions at $\sqrt{s} = 7$ TeV", *JHEP* **10** (2011) 132, doi:10.1007/JHEP10(2011)132, arXiv:1107.4789.

[39] CMS Collaboration, "The CMS trigger system", *JINST* **12** (2017) P01020, doi:10.1088/1748-0221/12/01/P01020, arXiv:1609.02366.

[40] CMS Collaboration, "Measurement of the properties of a Higgs boson in the four-lepton final state", *Phys. Rev. D* **89** (2014) 092007, doi:10.1103/PhysRevD.89.092007, arXiv:1312.5353.

[41] Particle Data Group, C. Patrignani et al., "Review of particle physics", *Chin. Phys C* **40** (2016) 100001, doi:10.1088/1674-1137/40/10/100001.

[42] J. Butterworth et al., "PDF4LHC recommendations for LHC Run II", *J. Phys. G* **43** (2016) 023001, doi:10.1088/0954-3899/43/2/023001, arXiv:1510.03865.

[43] NNPDF Collaboration, "Parton distributions for the LHC run II", *JHEP* **04** (2015) 040, doi:10.1007/JHEP04(2015)040, arXiv:1410.8849.

[44] CMS Collaboration, "CMS luminosity measurements for the 2016 data taking period", CMS Physics Analysis Summary CMS-PAS-LUM-17-001, CERN, 2017.